Appl Phys B (2009) 95: 559–563
DOI 10.1007/s00340-009-3486-z

Applied Physics B
Lasers and Optics

Hybrid nonlinearity supported by nonconventionally biased photorefractive crystals

P. Zhang · S. Liu · C. Lou · Y. Gao · J. Zhao · J. Xu · Z. Chen

Received: 1 December 2008 / Revised version: 27 February 2009 / Published online: 3 April 2009

Abstract We theoretically and experimentally demonstrate that a nonconventionally biased photorefractive crystal can support hybrid nonlinearity, i.e., coexistence of self-focusing and self-defocusing nonlinearities under an identical bias condition. It is revealed that the nonlinearity experienced by a one-dimensional (stripe) beam can be switched between self-focusing and self-defocusing solely by changing the beam orientation. For a two-dimensional beam, the hybrid nonlinearity leads to unusual nonlinear beam dynamics with enhanced anisotropy and nonlocality.

PACS 42.65.Jx · 42.65.Hw · 42.65.Tg

1 Introduction

Light wave propagation in nonlinear media has stimulated numerous theoretical and experimental research interests in the past few decades [1–3]. The nonlinear material response results in complex changes in the spatiotemporal structure of light, leading to a variety of intriguing nonlinear phenomena such as light-induced scattering [4], phase conjugation [5], and self-trapping [1–3, 6]. In fact, nearly all materials can exhibit perceptible nonlinearity at sufficient high light intensities, including crystals [7], liquids [8], and even gases [9]. Photorefractive crystal can exhibit relatively large nonlinearity at microwatt power levels, thus it became one of most popular materials for demonstrating nonlinear light dynamics during the past decades [10–12], in addition to other types of materials such as Kerr [8], saturable [9], and nonlocal [13] nonlinear materials. In general, the nonlinearities can be divided into two categories: self-focusing and self-defocusing nonlinearity. Although self-focusing and self-defocusing nonlinearities can be established by changing the polarity of the bias field in photorefractive crystals [14, 15], it remains a challenge to find a nonlinear material to support both nonlinearities simultaneously under an identical experimental setting, namely hybrid nonlinearity.

In a conventional setting of biased photorefractive crystals, the direction of the external field is set to be parallel to the crystalline c-axis [10–12, 14]. Therefore, the bias condition with a bias field along an arbitrary direction is named as the nonconventionally biased (NCB) condition [16–19]. In this paper, we demonstrate both in theory and experiment that a NCB photorefractive crystal can support hybrid nonlinearity. It is shown that the type of nonlinearity experienced by one-dimensional (1D) input beams could be self-focusing or self-defocusing depending on the beam orientation under an identical bias condition. While for two-dimensional (2D) cases, both self-focusing and self-defocusing nonlinearity will play a role during the nonlinear beam propagations, exhibiting enhanced anisotropy and nonlocality.

P. Zhang · S. Liu · Y. Gao · J. Zhao (✉)
Shaanxi Key Laboratory of Optical Information Technology, School of Science, Northwestern Polytechnical University, Xi'an 710072, China
e-mail: jlzhao@nwpu.edu.cn

C. Lou · J. Xu · Z. Chen
The Key Laboratory of Weak-Light Nonlinear Photonics, Ministry of Education and TEDA Applied Physics School, Nankai University, Tianjina 300457, China

Z. Chen
Department of Physics and Astronomy, San Francisco State University, San Francisco 94132, USA

2 Theoretical model

For a NCB photorefractive crystal, the direction of the external bias field is no longer parallel to the crystalline c-axis. The deformations of the index ellipsoids as well as the resultant refractive index changes for such crystals can be analyzed according to the linear electro-optic effect [20]. By using a SBN crystal as an example, it can be easily obtained that only the c-axis component of the bias field can introduce perceptible index modulation in the crystal, and the rotations of the c-axis and the refractive index changes introduced by the components of the bias field perpendicular to the c-axis can be neglected [17–21]. In addition, the bias field component parallel to the beam propagation direction cannot result in effective separation of the photo-excited electrons [21]. Therefore, it is reasonable to assume that the contribution of an NCB field is identical to that of its component perpendicular to the beam propagation direction. Here we consider an elliptical light beam propagating perpendicular to the crystalline c-axis with a polarization direction always parallel to the c-axis. A coordinate system is constructed by placing the x- and y-axis along the long and short principal axes of the elliptical beam profile, respectively, as shown in Fig. 1. The angles of the crystalline c-axis and the external bias field E_0 with respect to the x-axis are denoted by α and β, respectively. If the characteristic spatial scales are larger than the photorefractive Debye length, and the diffusion field can be neglected, the dimensionless equations determining the steady state propagation of a light beam in a NCB photorefractive crystal can be written as [17–19, 22]

$$\left(\frac{\partial}{\partial z}-\frac{i}{2}\nabla^2\right)B(\vec{r})=i\left(\frac{\partial\varphi}{\partial x}\cos\alpha+\frac{\partial\varphi}{\partial y}\sin\alpha\right)B(\vec{r}), \quad (1a)$$

$$\nabla^2\varphi+\nabla\varphi\cdot\nabla\ln(1+I) = E_0\left[\frac{\partial\ln(1+I)}{\partial x}\cos\beta+\frac{\partial\ln(1+I)}{\partial y}\sin\beta\right], \quad (1b)$$

where $\nabla=\hat{x}(\partial/\partial x)+\hat{y}(\partial/\partial y)$, $B(\vec{r})$is the amplitude of the optical field, φ is the light-induced electrostatic potential with the boundary condition $\nabla\varphi(\vec{r}\to\infty)\to 0$, and $I=|B(\vec{r})|^2$ is the normalized light intensity by the dark irradiance of the crystal (including background illumination).

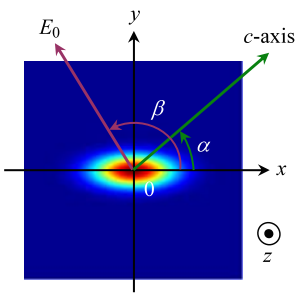

Fig. 1 Geometry of the coordinate system for nonconventionally biased photorefractive crystals

3 One-dimensional case

When the long axis of the elliptical beam depicted in Fig. 1 becomes infinite, (1) will degenerate into a 1D problem with $\partial\ln(1+I)/\partial x=0$ and $\partial\varphi/\partial x=0$. For a bright input beam, we can find the 1D analytical solution for (1b) reading as $\partial\varphi/\partial y=|E_0|I\sin\beta/(1+I)$. Therefore, the equation governing the nonlinear propagation of the 1D input beams becomes

$$\left(\frac{\partial}{\partial z}-\frac{i}{2}\frac{\partial^2}{\partial y^2}\right)B(y,z)=i|E_0|\sin\alpha\sin\beta\frac{I}{1+I}B(y,z). \quad (2)$$

Thus, the normalized light-induced refractive index changes can be described by $\Delta n=|E_0|I\sin\alpha\sin\beta/(1+I)$. Obviously, the type of the nonlinearity experienced by 1D input beams in NCB crystals depends on the values of α and β, i.e., the beam orientation relative to the crystalline c-axis and bias field. Now, we consider the nonlinearity versus the beam orientation under a fixed bias condition. Figure 2 depicts Δn versus α at different $(\beta-\alpha)$. It is obvious that, under the conventional bias condition $E_0//c$, the crystal can exhibit either a self-focusing nonlinearity ($\Delta n>0$) at $(\beta-\alpha)=0$ or a self-defocusing nonlinearity ($\Delta n<0$) at $(\beta-\alpha)=\pi$, but not both for a given $(\beta-\alpha)$. While for the NCB case at $(\beta-\alpha)=\pi/2$, for which the bias field is perpendicular to the crystalline c-axis ($E_0\perp c$), the crystal can exhibit self-focusing or self-defocusing nonlinearity depending on the beam orientation. That is to say, under such an NCB condition, if we launch two stripe beams respectively oriented at $\alpha=\pi/4$ and $-\pi/4$ into the crystal at same time, they will exhibit self-focusing and self-defocusing nonlinearity simultaneously in the same crystal under an identical bias condition (see Fig. 2). To visualize such hybrid nonlinearity by light propagations, we solve (2) with BPM. Figure 3 depicts the simulation results for the evolutions of an input 1D Gaussian beam $B(y)=\exp(-y^2/15)$ at different orientations relative to E_0 and c-axis, where the top to bottom rows correspond to $\alpha=0$, $-\pi/4$, and $\pi/4$, respectively, and the left and right panels correspond to the input beams and the evolution of the light intensity profiles along

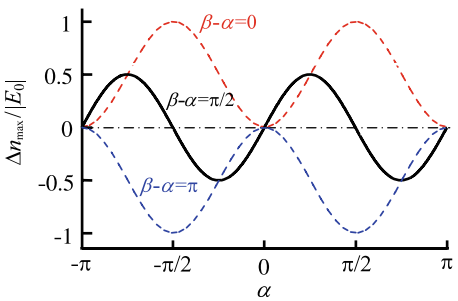

Fig. 2 1D light-induced refractive index changes (Δn) versus beam orientation (α) at different fixed bias conditions ($\beta-\alpha$)

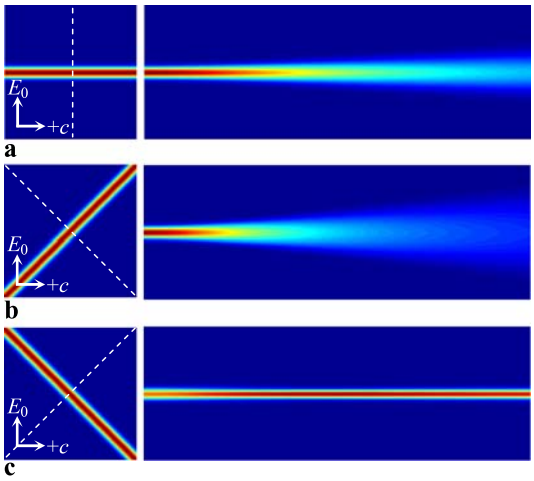

Fig. 3 BPM simulations on nonlinear propagations of 1D input beams at $\beta - \alpha = \pi/2$, but $\alpha = 0$ (**a**), $-\pi/4$ (**b**), and $\pi/4$ (**c**). *Left*: Input beam; *Right*: Evolution of the intensity profile along the *dashed line* in the *left panel*

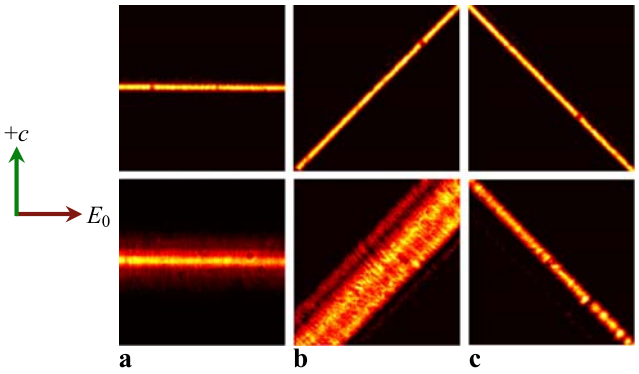

Fig. 4 Experimental results on nonlinear propagations of 1D input beams at $\beta - \alpha = \pi/2$, but $\alpha = 0$ (**a**), $-\pi/4$ (**b**), and $\pi/4$ (**c**), where the *top* (*bottom*) *panels* depict the intensity patterns of the input (output) beams

the dashed lines in the left panels. In our simulations, $E_0 = 1$ and the propagation length $z = 25$. As shown in Fig. 3(a), the input beam at $\alpha = 0$ cannot experience any nonlinearity; therefore, the input beam undergoes linear diffraction. From Figs. 3(a) and (b), we can see that the input beams at $\alpha = -\pi/4$ and $\alpha = \pi/4$ experience self-defocusing and self-defocusing nonlinearity, leading to enhanced diffraction and soliton-like propagation, respectively. Obviously, the simulation results coincide with our expectations from Fig. 2.

The experimental setup similar to that in [11] is used for our demonstrations. An expended and collimated laser beam ($\lambda = 532$ nm) is focused by a cylindrical lens to form a thin stripe beam as an input beam. The cylindrical lens, thus the beam orientation, can be rotated freely in the transverse plane. A SBN:60:Ce crystal sample with dimensions of $5 \times 5 \times 6.7(c)$ mm^3 and 0.1 wt.% dopant are used. The direction of the bias field (about 1.2 kV) is perpendicular to the crystalline c-axis, and both the amplitude and directions of the bias field are kept unchanged during our experiments. And the polarization direction of the input beam is always kept to be parallel to the crystalline c-axis. Figure 4 displays the typical experimental results corresponding to Fig. 3. Figures 4(a)–(c) correspond to the intensity patterns of the probe beam at input (top) and output (bottom). It is clear that the input beams indeed experience linear diffraction, self-defocusing, and self-focusing at different orientations under an identical bias condition. These experimental results are in good agreement with the theoretical results presented in Figs. 2 and 3.

4 Two-dimensional case

To solve (1b) in a 2D case, numerical procedures have to be employed. We use a Gaussian beam $B(\vec{r}) = \sqrt{2}\exp[-(x^2 + y^2)/16]$ as an input, which is depicted in Fig. 5(a). The light-induced refractive index changes under different bias conditions at $E_0 = 1$, having the form of $\frac{\partial\varphi}{\partial x}\cos\alpha + \frac{\partial\varphi}{\partial y}\sin\alpha$, are depicted in Figs. 5(b)–(d), where (b) and (c) correspond to the conventional case $E_0 // +c$ ($\alpha = \beta = 0$) and $E_0 // -c$ ($\alpha = \pi, \beta = 0$), respectively, and (d) corresponds to the typical NCB condition $E_0 \perp c$ ($\alpha = 0, \beta = \pi/2$). Figure 5(e) describes the linearly diffracted output beam pattern with a normalized propagation length $z = 15$. While the nonlinear output beam patterns under different bias conditions corresponding to Figs. 5(b)–(d) are depicted in Figs. 5(f)–(h), respectively. Figure 5(i) shows the FWHMs of the beam profiles along the dashed lines in Figs. 5(e) and (h) versus the propagation length z. From Fig. 5, we can see that different bias conditions will cause different index changes as well as various nonlinear beam propagations. Under conventional bias conditions, although the peripheral regions of the index changes possess opposite sign with respect to the central part, the nonlinearity experienced by the input beam is mainly determined by the index changes of the central part, resulting in self-focusing in Fig. 5(f) and self-defocusing in Fig. 5(g). While under the NCB condition at $E_0 \perp c$, the distribution of the index changes becomes very distinct in comparison with the conventional ones. From Fig. 5(d), it can be seen that the index change at the center of the input beam is zero, and the maxima of the index changes occur at the positions far away from the beam center, representing a typical nonlocality. More interestingly, along different diagonal directions across the beam center, the index changes always possess identical sign, but the sign and the maximum index changes can be dramatically different in different directions, representing an en-

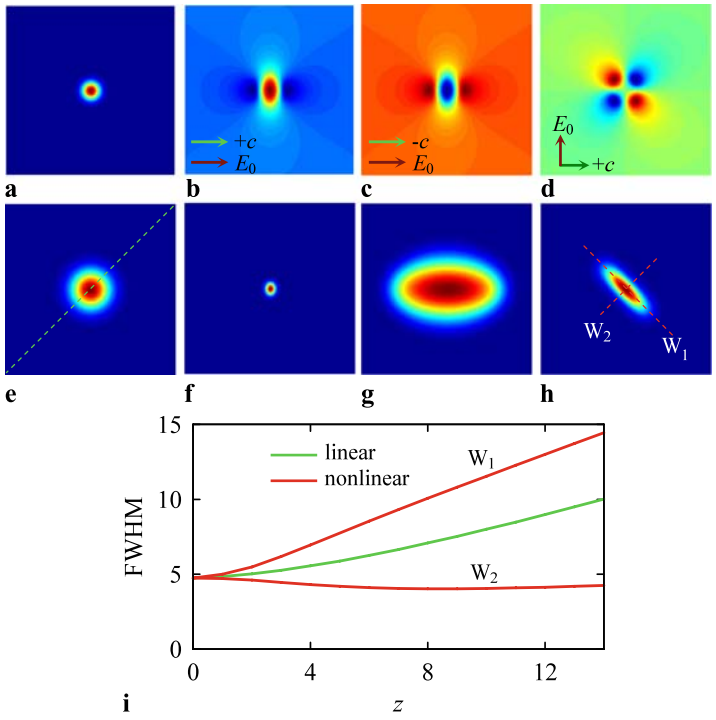

Fig. 5 Numerical simulations on 2D light-induced refractive index changes and nonlinear beam propagation, where (**a**) is the input beam, (**b**)–(**d**) are corresponding to the refractive index changes induced by (**a**) under different bias conditions indicated by the arrows, (**e**) is the output beam pattern after linear propagation, (**f**)–(**h**) depict the nonlinear output beam patterns under the same bias conditions with that in (**b**)–(**d**), and (**j**) depicts the FWHMs of the beams versus propagation length z along the dashed lines shown in (**e**) and (**h**)

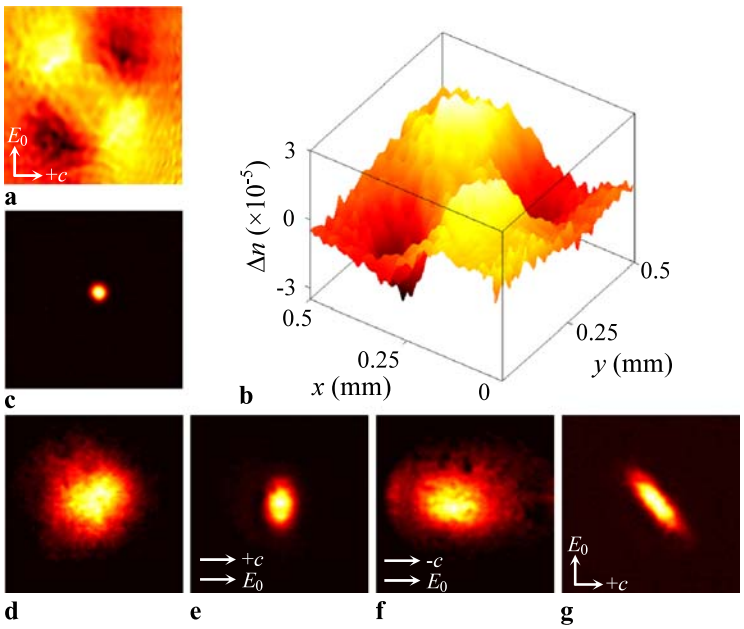

Fig. 6 Experimental results on 2D light-induced refractive index changes and nonlinear beam propagations. (**a**) and (**b**) depict the 2D and 3D displays of the measured refractive index changes at $E_0 \perp c$, corresponding to the center part of Fig. 5(d). (**c**)–(**g**) are the experimental results for beam propagations, where (**c**) is the input beam, and (**d**)–(**g**) are the linear and nonlinear output beam patterns corresponding to Figs. 5(e)–(h), respectively

hanced anisotropy. We can expect such unique features result in novel nonlinear beam propagation dynamics. From Figs. 5(h) and (i), it is clear that the input beam experiences self-focusing and self-defocusing at the same time, i.e., hybrid nonlinearity, leading to an elliptical output beam pattern.

To perform experimental demonstrations in a SBN crystal, we first directly visualize the index changes induced by a Gaussian beam at $E_0 \perp c$ by employing digital holography. The experimental setup is as same as that used in [19, 23]. The 2D and 3D display of the measured index changes are depicted in Figs. 6(a) and (b), respectively. For observing nonlinear beam propagation, we just replace the cylindrical lens with a circular lens in the setup for the 1D experiment described in Sect. 2. Figures 6(c)–(g) show the 2D experimental results, where (c) is the input beam pattern, and (d)–(g) are the linear and nonlinear output beam patterns corresponding to Figs. 5(e)–(h), respectively. By comparing Figs. 6 with 5, it is clear that our experimental results are in good agreement with the theoretical predictions.

5 Conclusions

We have demonstrated that a NCB photorefractive crystal can support hybrid nonlinearity. A theoretical model has been established to describe the nonlinear beam propagation in NCB photorefractive crystals. It has been shown that, for one-dimensional cases, the exhibited nonlinearity of the NCB photorefractive crystal depends on the orientation of the input beam. Solely by changing the input beam orientation, a switch between nonlinear self-focusing and self-defocusing can be obtained. While for two-dimensional cases, the hybrid nonlinearity will result in highly anisotropic and nonlocal refractive index modulations. Therefore, the input beam can experience self-focusing and self-defocusing nonlinearities at the same time, leading to an elliptical output beam profile. The experimental results agree well with our theoretical predictions. It should be noted that, in our previous work reported in [18, 19], we have focused on the novel soliton states in discrete regimes under NCB conditions, where the periodic nature of the induced photonic lattices plays a nontrivial role. However, the studies on the hybrid nonlinearity in homogeneous bulk samples should be of fundamental and general interest. Although we have studied elliptical solitons under NCB conditions in [17], the relation between the enhanced anisotropy/nonlocality and the hybrid nonlinearity was not studied in detail. Here we highlight the unique properties of the hybrid nonlinearity supported by the NCB photorefractive crystals. Such hybrid nonlinearity along with the enhanced anisotropy and nonlocality provide a good opportunity to explore novel nonlinear dynamics in continuum as well as discrete regimes, e.g., wave mixing, vortex evolution, optically induced soliton transitions from different bandgap, and 2D novel lattice soliton states, etc. Moreover, the novel concept of hybrid nonlinearity may have impacts on other nonlinear system beyond optics.

Acknowledgements This work was supported by the NPU Foundation for Fundamental Research, the Doctorate Foundation of NPU, the 973 program (2007CB613203), 111 project, NSFC, PCSIRT, NSF and AFOSR.

References

1. R.Y. Chiao, E. Garmire, C.H. Townes, Phys. Rev. Lett. **13**, 479 (1964)
2. H. Hasegawa, Y. Kodama, *Solitons in Optical Communications* (Oxford University, New York, 1995)
3. Y.S. Kivshar, G.P. Agrawal, *Optical Solitons: From Fibers to Photonic Crystals* (Academic, San Diego, 2003)
4. R.A. Rupp, F.W. Drees, Appl. Phys. B **39**, 223 (1986)
5. J. Feinberg, Opt. Lett. **7**, 486 (1982)
6. G.I. Stegeman, M. Segev, Science **286**, 1518 (1999)
7. M.D.I. Castillo, P.A. Marquez, J.J. Sanchez-Mondragon, S. Stepanov, V. Vysloukh, Appl. Phys. Lett. **64**, 408 (1994)
8. A. Barthelemy, S. Maneuf, C. Frcehly, Opt. Commun. **55**, 201 (1985)
9. J.E. Bjorkholm, A.A. Ashkin, Phys. Rev. Lett. **32**, 129 (1974)
10. M. Segev, B. Crosignanim, A. Yariv, B. Fischer, Phys. Rev. Lett. **68**, 923 (1992)
11. G.C. Duree Jr., J.L. Shultz, G. Salamo, M. Segev, A. Yariv, B. Crosignani, P. Di Porto, E.J. Sharp, R.R. Neurgaonkar, Phys. Rev. Lett. **71**, 533 (1993)
12. W. Królikowski, B. Luther-Davies, C. Denz, IEEE J. Quantum Electron. **39**, 3 (2003)
13. C. Rotschild, O. Cohen, O. Manela, M. Segev, T. Carmon, Phys. Rev. Lett. **95**, 213904 (2005)
14. M. Segev, G.C. Valley, B. Crosignani, D. Di Porto, A. Yariv, Phys. Rev. Lett. **73**, 3211 (1994)
15. D.N. Christodoulides, M.I. Carvalho, J. Opt. Soc. Am. B **12**, 1628 (1995)
16. C. Crognale, L. Rosa, J. Lightwave Technol. **23**, 2175 (2005)
17. P. Zhang, J. Zhao, C. Lou, X. Tan, Y. Gao, Q. Liu, D. Yang, J. Xu, Z. Chen, Opt. Express **15**, 536 (2007)
18. P. Zhang, S. Liu, J. Zhao, C. Lou, J. Xu, Z. Chen, Opt. Lett. **33**, 878 (2008)
19. P. Zhang, J. Zhao, F. Xiao, C. Lou, J. Xu, Z. Chen, Opt. Express **16**, 3865 (2008)
20. A. Yariv, P. Yeh, *Optical Waves in Crystals* (Wiley, New York, 1984)
21. P. Zhang, Y. Ma, J. Zhao, D. Yang, H. Xu, Appl. Opt. **45**, 2273 (2006)
22. A.A. Zozulya, D.Z. Anderson, Phys. Rev. A **51**, 1520 (1995)
23. J. Zhao, P. Zhang, J. Zhou, D.X. Yang, D.S. Yang, E. Li, Chin. Phys. Lett. **20**, 1748 (2003)